Applied Catalysis B: Environmental 201 (2017) 552–560

Contents lists available at ScienceDirect

Applied Catalysis B: Environmental

journal homepage: www.elsevier.com/locate/apcatb

Catalytic oxidation of 1,2-dichloropropane over supported $LaMnO_x$ oxides catalysts

Chuanhui Zhang[a,b,1], Chao Wang[a,b,1], Sonia Gil[b], Antoinette Boreave[b], Laurence Retailleau[b], Yanglong Guo[a,*], Jose Luis Valverde[c], Anne Giroir-Fendler[b,*]

[a] Key Laboratory for Advanced Materials and Research Institute of Industrial Catalysis, East China University of Science and Technology, Shanghai 200237, China

[b] Univ Lyon, Université Claude Bernard Lyon 1, CNRS, UMR 5256, IRCELYON, Institut de Recherches sur la Catalyse et l'Environnement de Lyon, 2 Avenue Albert Einstein, 69626, Villeurbanne Cedex, France

[c] Department of Chemical Engineering, University of Castilla-La Mancha, Avda. Camilo José Cela, 12, 13071 Ciudad Real, Spain

ARTICLE INFO

Article history:
Received 8 June 2016
Received in revised form 8 August 2016
Accepted 16 August 2016
Available online 17 August 2016

Keywords:
Chlorinated volatile organic compounds
Catalytic oxidation
Perovskite
Acidity
Oxygen mobility

ABSTRACT

$LaMnO_3$ perovskites supported on Al_2O_3, TiO_2, YSZ and CeO_2 were prospectively synthesized by the in situ citrate sol-gel method. The physicochemical properties of these prepared materials were characterized by XRD, N_2 sorption, H_2-TPR, O_2-TPD and NH_3-TPD. The catalytic performances of these materials were evaluated in the catalytic oxidation of 1,2-dichloropropane (1,2-DCP), which was selected as a model reaction for chlorinated volatile organic compounds (CVOCs) abatement. It was shown that $LaMnO_3$ perovskite structures were successfully formed over TiO_2 and YSZ (LMO/TiO_2 and LMO/YSZ), while just characteristic diffraction peaks assigned to oxide supports were observed over Al_2O_3 and CeO_2 supported catalysts (LMO/Al_2O_3 and LMO/CeO_2). The perovskites supported on TiO_2 and YSZ presented higher catalytic activities than the perovskite alone. However, catalyst LMO/CeO_2 exhibited an optimum catalytic behavior with high catalytic stability and durability for the oxidation of 1,2-DCP. Both the concentration of surface adsorbed oxygen species and the surface acidity were considered as the main factors responsible for the catalytic performances of these materials. Moreover, it was observed that oxygen mobility originated from the interaction of $LaMnO_3$ and/or $LaMnO_x$ phases with oxide supports could be an additional parameter influencing the catalytic performance.

1. Introduction

The atmospheric pollution has become a serious problem in recent years [1,2] due to the rapid development of the chemical industry and the increase of human activities, which is coincidental with the growing concern that population has for the environmental protection. As one of the main air pollutants, volatile organic compounds (VOCs), especially chlorinated volatile organic compounds (CVOCs), are greatly and directly released without any treatment, which not only increases the degree of atmosphere pollution, but also leads to harmful effects on public health. Among the current technologies for CVOCs abatement, catalytic oxidation has been considered as one of the most effective and promising technology due to its low operation temperature, high purification efficiency, recoverable heat and no secondary pollution. Three kinds of catalysts, namely supported precious metals [3–5], transition metal oxides [6–9] and zeolites [10–13], have been widely used in the catalytic oxidation of CVOCs. Among the transition metal oxides, perovskite-type metal oxides, more specifically $LaMnO_3$-based perovskites, have attracted much attention because they present suitable catalytic activity, high oxygen mobility and good thermal stability for the catalytic oxidation of various VOCs [14,15] and CVOCs [16–23]. Moreover, it has been demonstrated that the excellent properties of the oxide supports, such as the high specific surface area and good oxygen storage capacity as well as the electro-conductivity or acidity, could induce great interaction with $LaMnO_x$ species on the interface and inside the lattice, which can affect the total catalytic behavior of supported catalysts [24–27]. For example, an incipient formation of a $LaMnO_3$ perovskite structure with good dispersion at around 4–6% on ZrO_2 was necessary for the development of highly active sites in methane and CO oxidation [28]. Another literature reported that the porous zirconia as

* Corresponding authors.
E-mail addresses: ylguo@ecust.edu.cn (Y. Guo), anne.giroir-fendler@ircelyon.univ-lyon1.fr (A. Giroir-Fendler).

[1] Chuanhui Zhang and Chao Wang contributed equally to this work as co-first authors.

http://dx.doi.org/10.1016/j.apcatb.2016.08.038
0926-3373/

support not only enhanced the catalytic activity of bulk $LaMnO_3$ perovskite but also decreased the by-products formation in the total oxidation of chloromethane [29]. In our previous study, the $LaMnO_3$ perovskite phases interacting with TiO_2 and Y_2O_3–ZrO_2 (YSZ) oxides significantly affected both the oxygen mobility and catalytic activities for toluene oxidation. It was found that the supported catalysts exhibited a remarkable oxygen exchange activity and higher catalytic performances than the pure perovskite, which could be attributed to the abundant oxygen vacancies and oxygen ions on YSZ as well as the reducibility properties of titania (Ti^{4+}/Ti^{3+}) on TiO_2 [27].

In this work, 20 wt.% $LaMnO_3$ perovskite supported on different oxide supports were prepared by the in situ citrate sol-gel method [27]. Their catalytic activities were evaluated in the catalytic oxidation of 1,2-dichloropropane (1,2-DCP), which was selected as a model reaction for CVOCs abatement. The physicochemical properties of these catalysts including catalyst structure, chemical composition, reducibility, acidity and oxygen mobility were investigated by different characterization techniques.

2. Experimental

2.1. Preparation of supported $LaMnO_x$ oxides

The citrate route was used to prepare supported $LaMnO_x$ catalysts. Thus, $La(NO_3)_3{\cdot}6H_2O$ (Sigma Aldrich, >99.0%), $Mn(NO_3)_2{\cdot}4H_2O$ (Alfa Aesar, 98%) and citric acid (Alfa Aesar, >99.5%) used as precursors were completely dissolved in 25 mL distilled water. After keeping the solution at 80 °C for 10 min under magnetic stirring, the oxide support, such as Al_2O_3 (gamma, Rhodia), TiO_2 (Cristal), YSZ (8 mol% Y_2O_3 over ZrO_2, TOSOH) and CeO_2 (Rhône-Poulenc), which were previously pretreated at 750 °C in air for 2 h, was slowly added into the solution under agitation in order to prepare 20 wt.% $LaMnO_x$ supported catalysts. The formed material was continuously kept at 80 °C for 2 h to evaporate the excess amount of H_2O and then dried at 120 °C overnight. After the pretreatment in a muffle furnace at 200 °C (at a heating rate of 2 °C min^{-1}) for 1 h, the resulting material was finally calcined at 750 °C (at a heating rate of 5 °C min^{-1}) for 2 h in a quartz tubular reactor under air atmosphere. For comparison, pure $LaMnO_3$ perovskite oxide was prepared by using the same experimental procedure. The prepared catalysts containing Al_2O_3, TiO_2, YSZ and CeO_2 as supports were named to as LMO/Al_2O_3, LMO/TiO_2, LMO/YSZ and LMO/CeO_2, respectively.

2.2. Catalyst characterization

The chemical compositions of the different catalysts were quantitatively determined using inductively coupled plasma atomic emission spectroscopy (ICP-AES) on a flame Perkin Elmer M1100 spectrometer. Before the measurement, the metal oxides were dissolved using a mixture of inorganic acids (H_2SO_4, HNO_3 and HF).

Nitrogen sorption at low temperature (77 K) was performed on a Micromeritics Tristar 3000 surface area and porosity analyzer. Before the measurement, the samples were degassed at 300 °C for 3 h. The specific surface area (SSA) of each sample was quantitatively obtained by Brunauer-Emmett-Teller (BET) method.

Powder XRD patterns were recorded on a Bruker D5005 diffractometer equipped with a CuKα radiation (λ = 1.5418 Å) in the 2θ range of 10–80° with a step size of 0.05°.

Temperature-programmed reduction of hydrogen (H_2-TPR) was conducted on a self-designed setup equipped with a U-shaped quartz reactor and an INFICON IPC400 quadrupole mass spectrometer (MS). Prior to run, 100 mg of sample was pretreated in a pure oxygen stream at 500 °C for 30 min to achieve a complete oxidation. After cooling down to room temperature, 30 mL min^{-1} of 5 vol.% H_2/He gaseous mixture was introduced until the stabilization of MS baseline. Then, the reactor was heated at a ramp of 15 °C min^{-1} from room temperature to 930 °C. Simultaneously, the signal of consumed H_2 at m/e = 2 was recorded by the MS detector.

Temperature-programmed desorption of oxygen (O_2-TPD) was carried out on the same setup used to perform H_2-TPR. Prior to each test, gaseous oxygen was previously adsorbed by a pretreatment of the sample (100 mg) at 550 °C for 60 min under pure oxygen atmosphere. After cooling down to room temperature, the reactor was purged with 30 mL min^{-1} of pure helium until the stabilization of MS baseline. Then, the reactor was heated at a ramp of 15 °C min^{-1} from room temperature to 930 °C. Simultaneously, the signal of desorbed oxygen at m/e = 32 was recorded by the MS detector.

Temperature-programmed desorption of ammonia (NH_3-TPD) was performed on the same setup used to perform H_2-TPR and O_2-TPD. Firstly, the sample (100 mg) was pretreated in a nitrogen stream at 500 °C. After cooling down to 100 °C in the same atmosphere, ammonia adsorption was performed by introducing small flow of ammonia in helium at 100 °C up to saturation. Subsequently, the reactor was purged by 30 mL min^{-1} of pure helium at 100 °C until the stabilization of MS baseline in order to reversibly and physically remove adsorbed ammonia on the catalyst surface. Finally, the desorption was carried out from 100 to 800 °C at a ramp of 15 °C min^{-1} in helium stream (30 mL min^{-1}). Simultaneously, the signal of desorbed ammonia at m/e = 17 was recorded by the MS detector.

2.3. Catalyst testing

The measurement of the catalytic activity for the oxidation of 1,2-DCP was performed at atmospheric pressure in a conventional U-shaped tubular reactor placed into an electric furnace. 240 mg of the catalyst, mixed with a certain amount of silicon carbide (SiC) to avoid the occurrence of hot spots, was deposited on a quartz wool plug, and a thermocouple tied to the reactor was used to monitor the reaction temperature. A mixture of O_2, 1,2-DCP and He (20% O_2, 1000 ppm 1,2-DCP vapor and He balance) with a total flow rate of 60 mL min^{-1}, corresponding to a weight hourly space velocity (WHSV) of 15,000 mL g^{-1} h^{-1}, was fed to the catalytic bed. The concentration of 1,2-DCP was adjusted by a Calibrage PUL010 apparatus, which was constituted of a saturator and two helium streams controlled by mass flowmeters (Brooks). A helium stream was introduced into the saturator to maintain a constant flow rate of 1, 2-DCP vapor while the other one balanced. The reactor was heated from room temperature to 500 °C and kept for 1 h. Finally, it was cooled down to 100 °C. 1,2-DCP and possible organic products were analyzed by an Agilent 6850 network gas chromatography system with a flame ionization detector (FID). The conversion of 1,2-DCP (X_{DCP}) and selectivity of allyl chloride (AC, S_{AC}) were calculated according to the following equations:

$$X_{DCP}(\%) = \frac{[DCP]_{in} - [DCP]_{out}}{[DCP]_{in}} \times 100 \quad S_{AC}(\%) = \frac{[AC]_{out}}{[DCP]_{in}} \times 100$$

where $[DCP]_{in}$, $[DCP]_{out}$ and $[AC]_{out}$ were the inlet and outlet 1,2-DCP concentrations and the outlet AC concentration, respectively.

3. Results and discussions

3.1. Catalyst characterization

The physicochemical properties of the oxide supports, pure perovskite (catalyst $LaMnO_3$) and the supported catalysts are summarized in Table 1. ICP-AES analyses confirmed the presence of La and Mn in all the supported catalysts, expect for catalyst LMO/CeO_2.

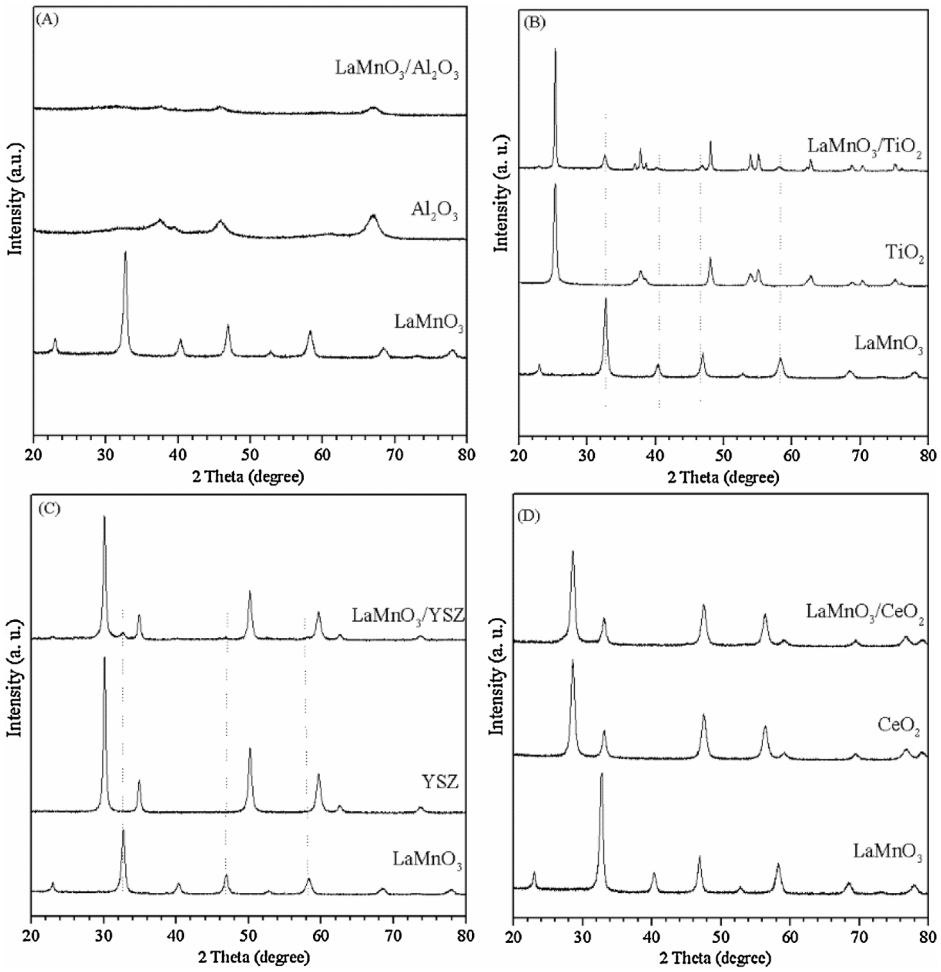

Fig. 1. XRD patterns of (A) $LaMnO_3$, Al_2O_3 and $LaMnO_3/Al_2O_3$, (B) $LaMnO_3$, TiO_2 and $LaMnO_3/TiO_2$, (C) $LaMnO_3$, YSZ and $LaMnO_3$/YSZ and (D) $LaMnO_3$, CeO_2 and $LaMnO_3/CeO_2$.

Table 1
Physicochemical properties of oxide supports and supported and pure $LaMnO_3$ catalysts.

Samples		Chemical compositions[a]		SSA[b] ($m^2\,g^{-1}$)	SSA[c] ($m^2\,g^{-1}$)	Crystal phases[d]
		La%	Mn%			
Supports	Al_2O_3	–	–	211	–	Gamma
	TiO_2	–	–	20	–	Rutile
	YSZ	–	–	14	–	Cubic
	CeO_2	–	–	77	–	Cubic
Catalysts	$LaMnO_3/Al_2O_3$	11.12 (11.49)[e]	4.00 (4.54)	172	175.8	Gamma
	$LaMnO_3/TiO_2$	12.07 (11.49)	4.26 (4.54)	23	23	Perovskite + Rutile
	$LaMnO_3$/YSZ	12.56 (11.49)	4.26 (4.54)	16	18.2	Perovskite + Cubic
	$LaMnO_3/CeO_2$	11.56 (11.49)	2.58 (4.54)	54	68.6	Cubic
	$LaMnO_3$	−(57.44)	−(22.72)	35	–	Perovskite

[a] Determined by ICP-AES analysis.
[b] Measured by N_2 sorption (BET method).
[c] Calculated according to the following equations: $SSA = 20\% \times SSA_{perovskite} + 80\% \times SSA_{support}$.
[d] Determined by XRD patterns (MDI Jade 5.0 program).
[e] The data in brackets are the nominal compositions of La and Mn in $LaMnO_3$.

The La/Mn molar ratio in each catalyst was closely fixed at the nominal value (La/Mn = 1). However, catalyst LMO/CeO_2 catalyst showed a loss of the Mn content (about 57%), which could be related to the presence of manganese oxide, which is not stable at high temperature. This hypothesis will be discussed later.

As shown in Table 1, Al_2O_3 and CeO_2 presented high surface specific areas (SSA): 211 and 77 $m^2\,g^{-1}$, respectively, while YSZ and TiO_2 showed much lower SSA values (14 and 20 $m^2\,g^{-1}$, respectively). $LaMnO_x$ species supported on the oxide supports with the highest SSA value (catalysts LMO/Al_2O_3 or LMO/CeO_2) also showed higher specific surface area than that the pure perovskite (35 $m^2\,g^{-1}$), but lower than that of corresponding support. Moreover, the SSA value of the supported perovskites was close to that evaluated by the weighted contribution of each specie (Table 1).

The presence of perovskite on the oxide supports was examined by XRD. XRD patterns of catalysts LMO/YSZ and LMO/TiO_2 showed the characteristic diffraction peaks assigned to the $LaMnO_3$ perovskite as well as those of the oxide support phases (Fig. 1B

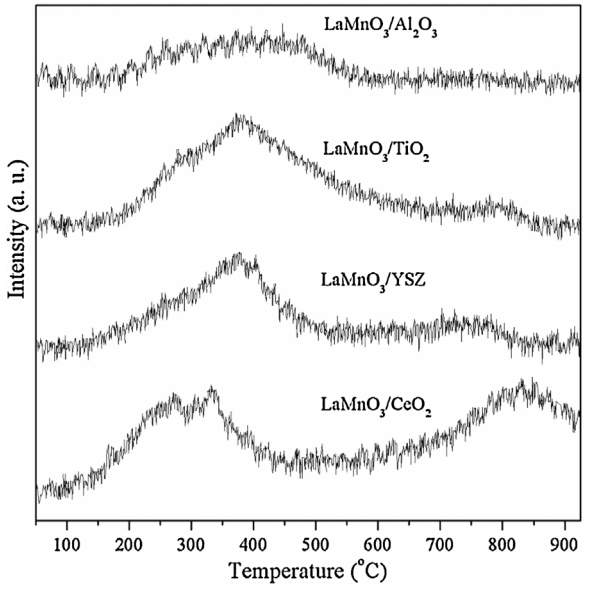

Fig. 2. H_2-TPR profiles of catalysts $LaMnO_3/Al_2O_3$, $LaMnO_3/TiO_2$, $LaMnO_3$/YSZ and $LaMnO_3/CeO_2$.

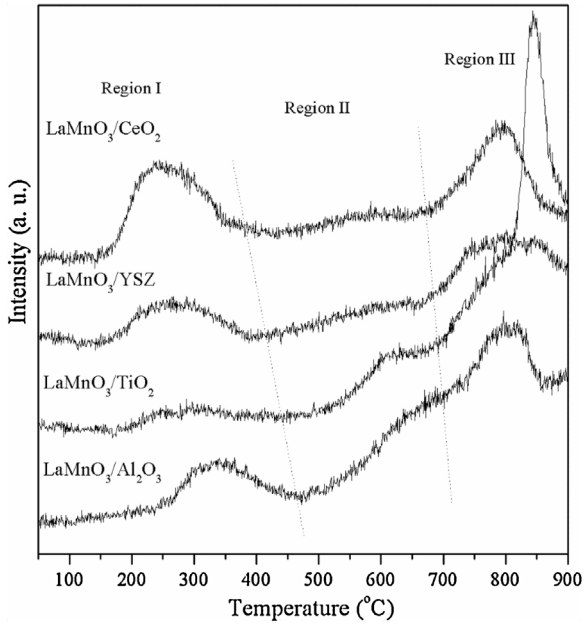

Fig. 3. O_2-TPD profiles of catalysts $LaMnO_3/Al_2O_3$, $LaMnO_3/TiO_2$, $LaMnO_3$/YSZ and $LaMnO_3/CeO_2$.

and C), which revealed that the preparation method and the further thermal treatment were suitable to create the crystallographic structure of these oxide supports, in turn allowing the formation of the $LaMnO_3$ perovskite structure. However, no characteristic diffraction peaks assigned to the $LaMnO_3$ perovskite structure were observed over catalysts LMO/Al_2O_3 and LMO/CeO_2. Regarding catalyst LMO/Al_2O_3, the temperature of the calcination step (750 °C) was close to the limit of the gamma alumina thermal stability, thus sample becoming amorphous (Fig. 1A). Anyway, the formation of perovskite structure was not favored on Al_2O_3 [30,31]. In the case of LMO/CeO_2, the calcination step preserved the crystallographic structure of cerium oxide (Fig. 1D). However, the perovskite structure was not clearly present and the content in manganese was lower than that observed for other samples. This could be associated to the La incorporation into the lattice of CeO_2, resulting in the formation of $Ce_{1-x}La_xO_2$ solid solution oxides [32]. This phenomenon could explain the loss of manganese (MnO_2 melting point is 535 °C) that could be formed in absence of lanthanum.

The H_2-TPR profiles of all the supported catalysts are plotted in Fig. 2 whereas the H_2 consumption related to each reduction region calculated through quantitative integration of the corresponding TPR peaks is listed in Table 2. All the catalysts showed one and/or two reduction peaks at the low temperature region (100–550 °C) and, in some cases, a peak at the high temperature region (>550 °C), which were ascribed to the reduction of different species. Herein, catalyst LMO/Al_2O_3 exhibited a single reduction peak at the low temperature region, which could be associated with the reduction of both the surface adsorbed oxygen species and Mn^{4+} into Mn^{3+}. Moreover, the low intensity and broad width of the latter peak could be attributed to the interaction between manganese ions and Al_2O_3, probably hindering the reduction process of Mn^{4+} into Mn^{3+}, which resulted in low H_2 consumption (0.6872 mmol g^{-1}).

For the rest of catalysts, two reduction peaks at the low temperature region were present, showing higher intensity than that of catalyst LMO/Al_2O_3. This fact would indicate that more reducible species were available on the catalyst surface, leading to a higher reduction rate and, consequently, a higher H_2 consumption. Moreover, as previously reported [33], reduction of TiO_2 could not be completed at temperatures lower than 650 °C. Regarding catalyst LMO/TiO_2, the two reduction peaks occurring at the low temperature region (centered at 290 and 382 °C), leading to the highest H_2 consumption of 1.2734 mmol g^{-1}, could be assigned to the reduction of both surface oxygen and Mn^{4+} into Mn^{3+}. In addition, the second peak occurring at the low temperature region could be attributed not only to the reduction of the perovskite phase but also to the partial reduction of TiO_2 (Ti^{4+} into Ti^{3+}) [21,23,28,34]. On the other hand, a small peak centered at 780 °C with a H_2 consumption of 0.0756 mmol g^{-1} was observed, corresponding to the further reduction of TiO_2 and Mn^{3+} into Mn^{2+}.

Catalyst LMO/YSZ exhibited a similar reduction profile as catalyst LMO/TiO_2 (H_2 consumptions of 0.7765 and 0.1281 mmol g^{-1} corresponding to the low-temperature and high-temperature regions, respectively). The total H_2 consumption could be associated to the reduction of both surface oxygen species and Mn^{4+} into Mn^{2+}, without any contribution of the YSZ support because of its high thermal stability [35].

Finally, the TPR profile of catalyst LMO/CeO_2 presented two peaks at the low temperature region. The former could be ascribed to the reduction of surface adsorbed oxygen species and well-dispersed MnO_x species whereas the latter could be attributed to the reduction of MnO_x incorporated into CeO_2 lattice in the form of $Ce_{1-x}Mn_xO_2$ solid solution [36,37]. In addition, the average reduction temperature of this catalyst was lower than that of other catalysts, which revealed the higher reducibility of this catalyst. Regarding the high temperature region, a reduction peak centered at 825 °C with the most H_2 consumption of 0.5884 mmol g^{-1} was observed, which could be ascribed to the reduction of released lattice oxygen as well as the reduction of both Mn^{3+} into Mn^{2+} and Ce^{4+} into Ce^{3+}.

In order to investigate the nature and location of surface and bulk oxygen species as well as their mobility, O_2-TPD was performed. As shown in Fig. 3, the oxygen desorption profiles presented two regions ranging from 100 to 450 °C (Region I) and from 450 to 900 °C (Region II), respectively. For all the catalysts, the desorbed oxygen in Region I could be ascribed to the surface adsorbed molecular oxygen and/or oxygen species migrating via surface oxygen vacancies [38–40].

The desorbed oxygen amounts based on the quantitative integration of O_2-TPD profiles are summarized in Table 2. Catalyst LMO/TiO_2 exhibited the lowest desorption intensity in Region I

Table 2
H_2 consumption and amounts of desorbed NH_3 and O_2 over catalysts $LaMnO_3/Al_2O_3$, $LaMnO_3/TiO_2$, $LaMnO_3$/YSZ and $LaMnO_3/CeO_2$, respectively.

Catalysts	H_2 consumption (mmol g^{-1})		Desorbed O_2 (mmol g^{-1})			Desorbed NH_3 (mmol g^{-1})	
	Low-temperature	High-temperature	R.I	R.II	R.III	Weak	Strong
$LaMnO_3/Al_2O_3$	0.6872	0.0064	0.0086	0.0207	0.0377	0.0684	0.0050
$LaMnO_3/TiO_2$	1.2734	0.0756	0.0028	0.0102	0.0403	0.0013	–
$LaMnO_3$/YSZ	0.7765	0.1281	0.0085	0.0083	0.0166	0.0122	–
$LaMnO_3/CeO_2$	0.8256	0.5884	0.0170	0.0043	0.0154	0.0364	–

(0.0028 mmol g^{-1} of desorbed oxygen), which could be associated to the low oxygen mobility and the minimum amount of surface oxygen species present on this catalyst, which could be in turn related to its relatively low specific surface area and lack of surface oxygen vacancies [28]. Despite the lower specific surface area of catalyst LMO/YSZ (15.5 m^2 g^{-1}) if compared to that of catalyst LMO/Al_2O_3 (172.1 m^2 g^{-1}), the former exhibited a higher desorption intensity, a lower desorption temperature and nearly equal quantity of desorbed oxygen in Region I than the latter (0.0086 and 0.0085 mmol g^{-1}, respectively). As it is well known, YSZ is a good ionically conducting material with superior oxygen vacancy property [28,29,41], where oxygen vacancy should be considered as the key factor for oxygen migration and desorption. Finally, catalyst LMO/CeO_2 presented the most intense desorption signal, the lowest desorption temperature and the highest amount of desorbed oxygen in Region I (0.0170 mmol g^{-1}), indicating its superior oxygen mobility and high concentration of surface oxygen. This could be attributed to (i) its high specific surface area (53.5 m^2 g^{-1}); (ii) its good oxygen storage capacity (OSC) of the CeO_2 support [42], resulting in more available surface oxygen species; and (iii) the high amount of oxygen vacancies present on the catalyst surface due to the formation of a $Ce_{1-x}Mn_xO_2$ solid solution, which could improve the oxygen mobility.

Additionally, Region II could be divided into two desorption peaks corresponding to the ranges from 450 to 700 °C and from 700 to 900 °C. On one hand, the oxygen species desorbed corresponding to the first desorption peak could be ascribed to the oxygen species migrating from the subsurface of $LaMnO_3$ or $LaMnO_x$ phases and the interface between these phases and the corresponding supports [38–40]. Among them, catalyst LMO/Al_2O_3 possessed the highest amount of desorbed oxygen (0.0207 mmol g^{-1} if compared to that of catalyst LMO/CeO_2 which resulted to be 0.0043 mmol g^{-1}). This fact could be associated with the high specific surface area of the Al_2O_3 support. On the other hand, the oxygen species desorbed in the second desorption peak could be linked to lattice oxygen, whose migration and desorption should be achieved at even high temperature [38–40]. The amount of desorbed oxygen followed the sequence: LMO/TiO_2 (0.0403 mmol g^{-1}) > LMO/Al_2O_3 (0.0377 mmol g^{-1}) > LMO/YSZ (0.0166 mmol g^{-1}) > LMO/CeO_2 (0.0154 mmol g^{-1}). It should be noted that catalyst LMO/TiO_2 exhibited the highest amount of desorbed oxygen (an intense peak centered at 845 °C), which indicated that the release of lattice oxygen over TiO_2 was easier if compared to that of other supports.

It is well known that the acidity of catalysts is another factor to influence the catalytic activity for CVOCs oxidation [43–49]. With this purpose, NH_3-TPD was performed, where NH_3 was selected as the probe molecule to determine acid strength and amounts of acid sites. As shown in Fig. 4, the NH_3-TPD profiles could be divided into two regions [46] according to the temperature range of NH_3 desorption. The low temperature one, ranging from 100 to 500 °C, corresponded to weak-strength acid sites and was present for all the catalysts tested. The high temperature one, for peaks appearing at temperatures higher that 500 °C, assigned to the strong-strength acid sites was only detected for catalyst LMO/Al_2O_3, which was associated to the superior acidity nature of the Al_2O_3 support. Catalysts LMO/TiO_2 and LMO/YSZ catalysts exhibited low weak-strength acidity (Table 2), whereas catalysts LMO/Al_2O_3 and LMO/CeO_2 showed an intense desorption peak associated to weak-strength acidy.

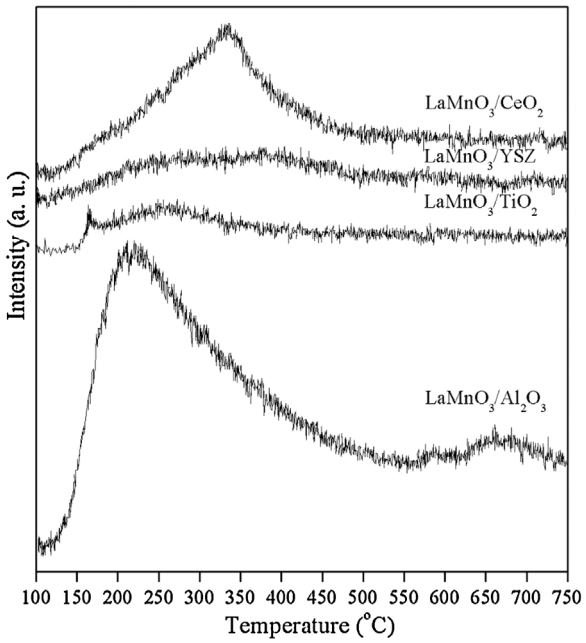

Fig. 4. NH_3-TPD profiles of catalysts $LaMnO_3/Al_2O_3$, $LaMnO_3/TiO_2$, $LaMnO_3$/YSZ and $LaMnO_3/CeO_2$.

3.2. Catalytic activity in the 1,2-DCP oxidation

Firstly, the supports used in this study (Al_2O_3, TiO_2, YSZ and CeO_2) were tested as catalysts in the oxidation of 1,2-DCP. Fig. 5 shows the 1,2-DCP conversion and the allyl chloride (AC) selectivity as a function of reaction temperature over different supports during the cooling ramp. Allyl chloride was the main intermediate obtained as a result of the dechlorination reaction of 1,2-DCP [17,50,51].

A preliminary blank test without any catalyst was performed in order to ensure that the kinetic experiments provided meaningful results. It was shown that 46% of 1,2-DCP was converted at a reaction temperature of 530 °C. This specie was not completely oxidized to CO_x, H_2O and HCl at this high temperature but AC was also formed (selectivity to this compound equal to 32%) (Fig. 5A and B), clearly indicating that the presence of a catalyst was required for effectively completing the dehydrochlorination process.

The sequence of decreasing activity (Fig. 5A), and AC selectivity (Fig. 5B), of the different supports here tested for the complete oxidation of 1,2-DCP was the next one: CeO_2 > TiO_2 > Al_2O_3 > YSZ. The complete oxidation of both 1,2-DCP and AC was reached above 500 °C for all the supports but YSZ. Moreover, the maximum of the peak of AC formation was reached at practically the same temperature as the total conversion of 1,2-DCP was attained, which would indicate that the catalytic oxidation of 1,2-DCP was performed in

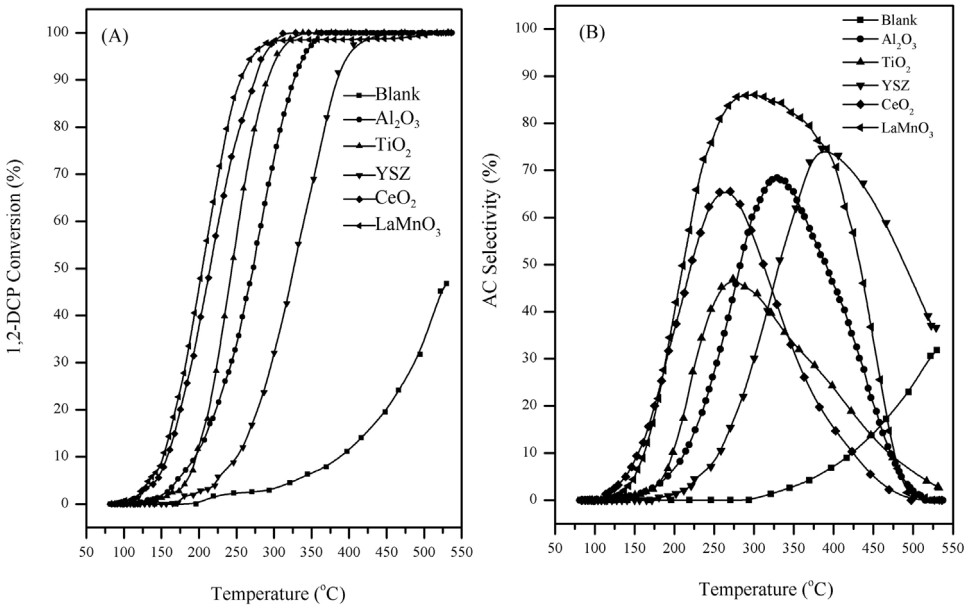

Fig. 5. (A) 1, 2-DCP conversion and (B) AC selectivity as a function of reaction temperature over oxide supports.

Table 3
T_{50}, T_{90} and $T_{AC=0}$ corresponding to 50%, 90% of 1,2-DCP conversion and zero yield of AC in the catalytic oxidation of 1,2-DCP.

Catalysts	T_{50} (°C)	T_{90}(°C)	$T_{AC=0}$ (°C)
Al_2O_3	270	325	510
$LaMnO_3/Al_2O_3$	178	243	460
TiO_2	243	291	–
$LaMnO_3/TiO_2$	183	249	507
YSZ	326	383	–
$LaMnO_3$/YSZ	189	243	460
CeO_2	215	274	500
$LaMnO_3/CeO_2$	171	260	440

two steps: (i) dehydrochlorination of 1,2-DCP into AC at relatively low temperature, and (ii) further oxidation of AC into CO_x, H_2O and HCl at high temperature. The first step readily occurred on the surface acid sites whereas the second one required the presence of redox sites, as reported Sinquin et al. [17,52]. These results showed that the oxide supports influence the catalytic performances in the oxidation of 1,2-DCP, which could be correlated to their physicochemical properties. Thus, the highest catalytic activity of the CeO_2 support could be attributed to its high oxygen storage capacity and the presence of a high amount of surface acid sites, whereas the high catalytic activity of Al_2O_3 could be associated with the high acidity and specific surface area of this support [17,46–49]. However, TiO_2 and YSZ supports, with lower specific surface areas and lower amount of acid sites, presented relatively lower oxidation activities. Summarizing, the specific surface area, the oxygen storage capacity and the surface acid sites of the simple oxide supports would be the main parameters to influence their catalytic performances for the oxidation of 1,2-DCP.

Fig. 6 shows the 1,2-DCP conversion and the AC selectivity as a function of reaction temperature over the pure $LaMnO_3$ and derived catalysts during the cooling ramp. Table 3 lists the reaction temperatures corresponding to 50% (T_{50}), 90% (T_{90}) of 1,2-DCP conversion and the zero yield of AC ($T_{AC=0}$, meaning a complete oxidation of both 1,2-DCP and AC into final products). All the supported catalysts presented higher catalytic activities than the oxides supports and the pure perovskite. It can be seen that the curves of 1,2-DCP conversion were nearly overlapped among them for all supported catalysts (Fig. 6A), thus meaning that the $LaMnO_3$ and/or $LaMnO_x$ species on the oxide supports should significantly improve the catalytic performance for the oxidation of 1,2-DCP. Anyway, the catalytic activity for the complete oxidation of 1,2-DCP and AC (Fig. 6B) was a function of the nature of the oxides supports. This could be attributed to the reducibility, the oxygen capacity and mobility of both species as well as the interaction between them [17,50,52,53]. Obviously, catalyst LMO/CeO_2 with the best low-temperature reducibility, the highest surface adsorbed oxygen capacity and the most abundant surface acid sites presented the highest catalytic activity for the oxidation of 1,2-DCP and AC into final products, which was achieved at 440 °C. It should be noted that catalyst LMO/YSZ presented similar redox properties but lower both specific surface area and acidity than the catalyst supported on Al_2O_3. However, these catalysts showed a similar catalytic performance for the complete oxidation of 1,2-DCP and AC, which was achieved at 460 °C. This fact was related to the high amount of oxygen vacancies on YSZ support, which could improve the oxygen mobility, the diffusion and the activation of oxygen from the $LaMnO_3$-YSZ interface [28]. Thus, the surface active oxygen species could be continuously supplemented and participated in the oxidation of 1,2-DCP. Catalyst LMO/TiO_2 presented the lowest catalytic activity, but a little bit higher than that of $LaMnO_3$, thus leading to the complete oxidation of 1,2-DCP and AC at similar temperature (above 500 °C), which could be attributed to the lack of surface active oxygen species and the low amount of surface acid sites present on the catalyst. Summarizing, these results confirmed that not only the surface acid sites but also the redox sites were needed for the complete removal of chlorinated organic compounds.

3.3. Catalytic stability in the 1,2-DCP oxidation

Three consecutive catalytic runs were performed by using catalyst LMO/CeO_2, which could considered, according to the above discussion, as the optimum one. Fig. 7 displays the corresponding curves of 1,2-DCP conversion and AC selectivity during the cooling ramp after three consecutive runs. No appreciable deactivation was detected after them; 1,2-DCP conversion curves were overlapped each other within the experimental error (±5 °C). AC selectivity decrease after the three consecutive runs, whereas the temperature at which the complete oxidation of 1,2-DCP and AC was achieved remained practically constant.

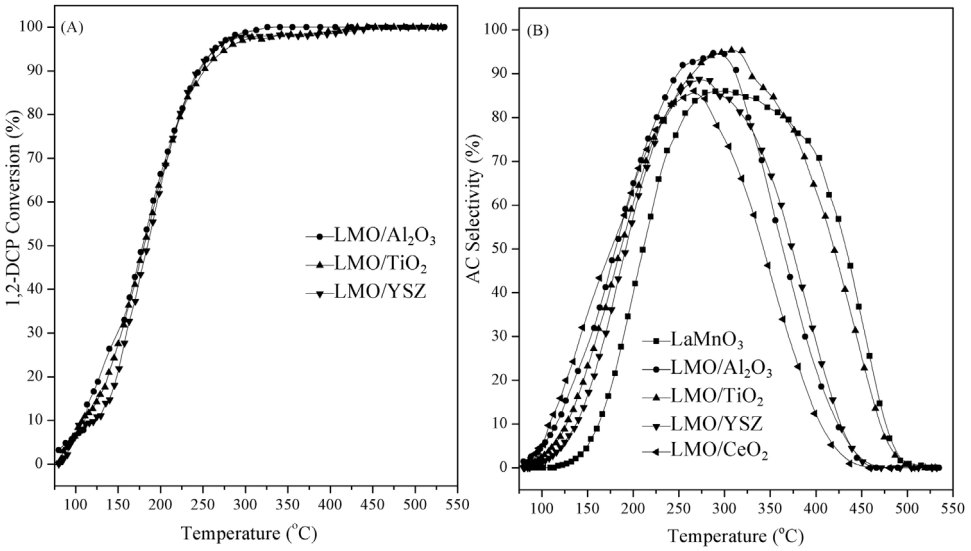

Fig. 6. (A) 1, 2-DCP conversion and (B) AC selectivity as a function of reaction temperature over supported $LaMnO_3$ catalysts.

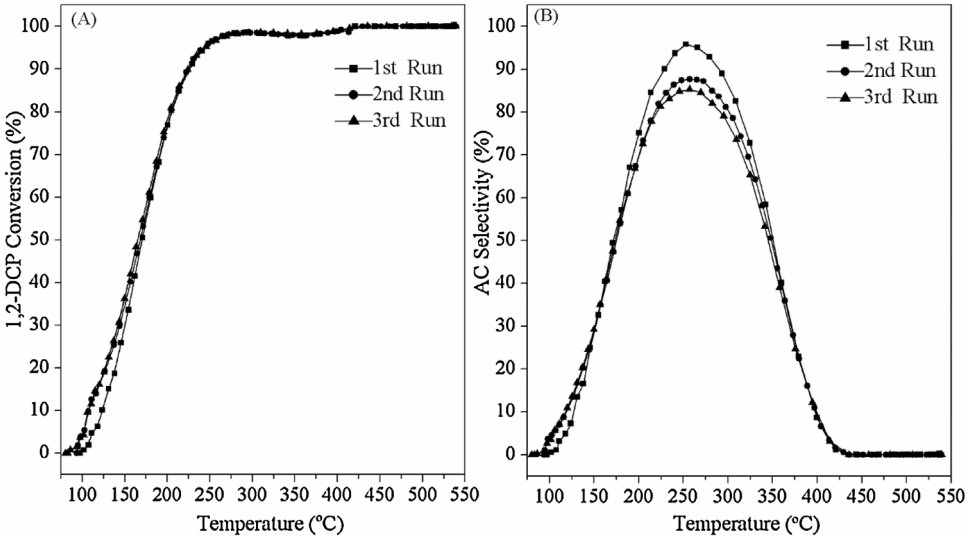

Fig. 7. (A) 1,2-DCP conversion and (B) AC selectivity as a function of reaction temperature for 1, 2-DCP oxidation in three consecutive runs over catalyst $LaMnO_3/CeO_2$.

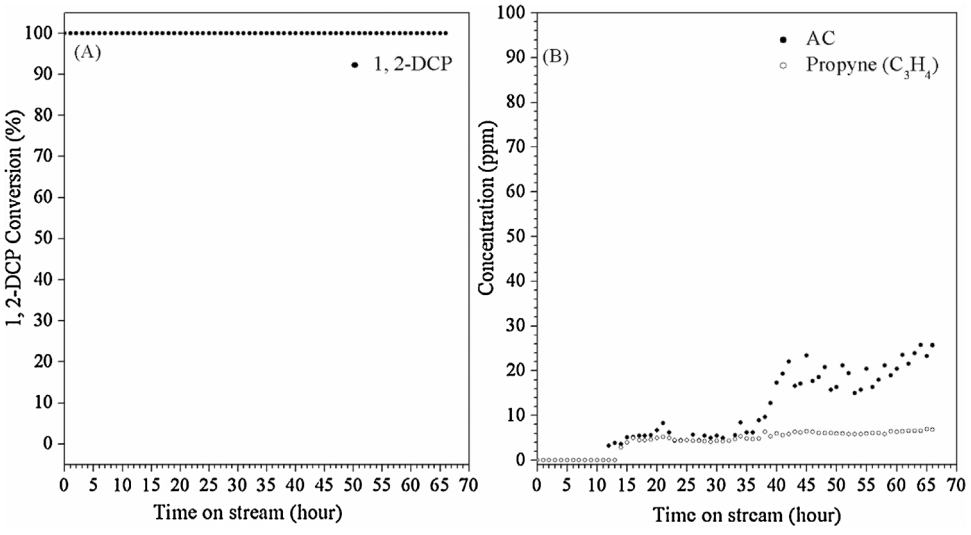

Fig. 8. (A) 1,2-DCP conversion and (B) concentrations of reaction intermediates as a function of time on stream over catalyst $LaMnO_3/CeO_2$ at 450 °C.

In addition, a durability test for the oxidation of 1,2-DCP over catalyst LMO/CeO_2 was carried out for 66 h at the reaction temperature of 450 °C. The 1,2-DCP conversion and the intermediates concentrations versus the time on stream are shown in Fig. 8. Complete conversion of 1,2-DCP was always observed during the entire reaction time, confirming the stable catalytic performance of the catalyst tested. Moreover, during the first 12 h, no intermediates were detected, indicating that 1,2-DCP was completely oxidized into CO_x, H_2O and HCl. However, traces of AC and propyne (C_3H_4), as the main reaction intermediates, were detected after 12 and 14 h on stream. The concentrations of propyne and AC remained constant (about 6 ppm) during the entire test period and the first 35 h, respectively. Afterwards, AC concentration increased until 26 ppm. In conclusion, good catalytic stability and durability was confirmed with the optimum catalyst during three consecutive runs and long-term experiments.

4. Conclusions

In this work, $LaMnO_x$ supported on different oxide supports (Al_2O_3, TiO_2, YSZ and CeO_2) was prepared by in situ citrate sol-gel method and characterized by several techniques. Their catalytic performances and stability were evaluated for the catalytic oxidation of 1,2-DCP. As derived from catalyst characterizations and catalytic tests, the following conclusions can be obtained:

(i) The $LaMnO_3$ perovskite phase was successfully synthesized on TiO_2 and YSZ supports, whereas only the characteristic diffraction peaks assigned to oxide supports were observed on Al_2O_3 and CeO_2.
(ii) The oxide support had an important influence on the acid and redox properties of the catalyst and, consequently, on the catalytic activity for the oxidation of 1,2-DCP.
(iii) The supported catalysts presented higher catalytic activity and AC selectivity than the corresponding oxide supports, which indicated that the growing presence of $LaMnO_x$ species improved the catalytic performances.
(iv) Catalyst LMO/CeO_2 showed the highest catalytic activity for the oxidation of 1,2-DCP. The complete oxidation of 1,2-DCP and AC was achieved at 440 °C. In addition, its good catalytic stability was confirmed during three consecutive runs and long-term experiments.
(v) The concentration of surface adsorbed oxygen species and surface acid sites were considered as the responsible of the catalytic performance of supported catalysts. Furthermore, the oxygen mobility originated from the interaction between $LaMnO_3$/$LaMnO_x$ species and oxide supports could be another parameter to influence the catalytic performance.
(vi) Finally, the highest oxidation performance of catalyst LMO/CeO_2 could be associated with the presence of a high amount of active acid sites, which would favor the dehydrochlorination of 1,2-DCP into AC, as well as the higher oxygen storage capacity, which would promote the further oxidation by surface active oxygen from the ceria support.

Acknowledgements

This work was financially supported by the "Région Rhône Alpes" (Coopera project 113955/2015), the National Key Research and Development Program of China (2016YFC0204300), the National Natural Science Foundation of China (21577035), the Commission of Science and Technology of Shanghai Municipality (15DZ1205305) and 111 project (B08021). Thanks are also due to China Scholarship Council for the joint Ph.D. Program with Institute de recherches sur la catalyse et l'environnement de Lyon (IRCELYON), Centre national de la recherche scientifique (CNRS) and Université Claude Bernard Lyon 1 (UCBL1).

Appendix A. Supplementary data

Supplementary data associated with this article can be found, in the online version, at http://dx.doi.org/10.1016/j.apcatb.2016.08.038.

References

[1] Y. Wang, H. Xu, H. Shang, M. Gong, Y. Chen, Excellent complete conversion activity for methane and CO of Pd/TiO_2–$Zr_{0.5}Al_{0.5}O_{1.75}$ catalyst used in lean-burn natural gas vehicles, J. Energy Chem. 23 (2014) 461–467.
[2] J. Tang, K. Chu, L. Chan, Y. Chen, Non-methane hydrocarbon emission profiles from printing and electronic industrial processes and its implications on the ambient atmosphere in the Pearl River Delta, South China, Atmos. Pollut. Res. 5 (2014) 151–160.
[3] M. Paulis, L.M. Gandıía, A. Gil, J. Sambeth, J.A. Odriozola, M. Montes, Influence of the surface adsorption–desorption processes on the ignition curves of volatile organic compounds (VOCs) complete oxidation over supported catalysts, Appl. Catal. B 26 (2000) 37–46.
[4] L. Wang, M. Sakurai, H. Kameyama, Catalytic oxidation of dichloromethane and toluene over platinum alumite catalyst, J. Hazard. Mater. 154 (2008) 390–395.
[5] A. Koyer-Gołkowska, A. Musialik-Piotrowska, J.D. Rutkowski, Oxidation of chlorinated hydrocarbons over Pt–Pd-based catalyst: part 1. Chlorinated methanes, Catal. Today 90 (2004) 133–138.
[6] X. Ma, X. Feng, J. Guo, H. Cao, X. Suo, H. Sun, M. Zheng, Catalytic oxidation of 1,2-dichlorobenzene over Ca-doped FeO_x hollow microspheres, Appl. Catal. B 147 (2014) 666–676.
[7] N. Blanch-Raga, M.D. Soriano, A.E. Palomares, P. Concepción, J. Martínez-Triguero, J.M.L. Nieto, Catalytic abatement of trichloroethylene over Mo and/or W-based bronzes, Appl. Catal. B 130–131 (2013) 36–43.
[8] V.H. Vu, J. Belkouch, A. Ould-Dris, B. Taouk, Removal of hazardous chlorinated VOCs over Mn–Cu mixed oxide based catalyst, J. Hazard. Mater. 169 (2009) 758–765.
[9] Y. Dai, X. Wang, Q. Dai, D. Li, Effect of Ce and La on the structure and activity of MnO_x catalyst in catalytic combustion of chlorobenzene, Appl. Catal. B 111–112 (2012) 141–149.
[10] M. Gallastegi-Villa, M. Romero-Sáez, A. Aranzabal, J.A. González-Marcos, J.R. González-Velasco, Strategies to enhance the stability of h-bea zeolite in the catalytic oxidation of Cl-VOCs: 1,2-dichloroethane, Catal. Today 213 (2013) 192–197.
[11] R. López-Fonseca, J.I. Gutiérrez-Ortiz, J.R. González-Velasco, Catalytic combustion of chlorinated hydrocarbons over H-BETA and PdO/H-BETA zeolite catalysts, Appl. Catal. A 271 (2004) 39–46.
[12] L. Pinard, P. Magnoux, P. Ayrault, M. Guisnet, Oxidation of chlorinated hydrocarbons over zeolite catalysts 2. Comparative study of dichloromethane transformation over NaX and NaY zeolites, J. Catal. 221 (2004) 662–665.
[13] M. Guillemot, J. Mijoin, S. Mignard, P. Magnoux, Mode of zeolite catalysts deactivation during chlorinated VOCs oxidation, Appl. Catal. A 327 (2007) 211–217.
[14] R. Spinicci, M. Faticanti, P. Marini, S. De Rossi, P. Porta, Catalytic activity of $LaMnO_3$ and $LaCoO_3$ perovskites towards VOCs combustion, J. Mol. Catal. A: Chem. 197 (2003) 147–155.
[15] Z.-J. Sui, L. Vradman, I. Reizner, M.V. Landau, M. Herskowitz, Effect of preparation method and particle size on $LaMnO_3$ performance in butane oxidation, Catal. Commun. 12 (2011) 1437–1441.
[16] K. Poplawski, J. Lichtenberger, F.J. Keil, K. Schnitzlein, M.D. Amiridis, Catalytic oxidation of 1,2-dichlorobenzene over ABO_3-type perovskites, Catal. Today 62 (2000) 329–336.
[17] G. Sinquin, C. Petit, J.P. Hindermann, A. Kiennemann, Study of the formation of $LaMO_3$ (M = Co, Mn) perovskites by propionates precursors: application to the catalytic destruction of chlorinated VOCs, Catal. Today 70 (2001) 183–196.
[18] G. Sinquin, C. Petit, S. Libs, J.P. Hindermann, A. Kiennemann, Catalytic destruction of chlorinated C_1 volatile organic compounds (CVOCs) reactivity, oxidation and hydrolysis mechanisms, Appl. Catal. B 27 (2000) 105–115.
[19] G. Sinquin, C. Petit, S. Libs, J.P. Hindermann, A. Kiennemann, Catalytic destruction of chlorinated C_2 compounds on a $LaMnO_{3+\delta}$ perovskite catalyst, Appl. Catal. B 32 (2001) 37–47.
[20] C. Zhang, W. Hua, C. Wang, Y. Guo, Y. Guo, G. Lu, A. Baylet, A. Giroir-Fendler, The effect of A-site substitution by Sr, Mg and Ce on the catalytic performance of $LaMnO_3$ catalysts for the oxidation of vinyl chloride emission, Appl. Catal. B 134–135 (2013) 310–315.
[21] C. Zhang, C. Wang, W. Zhan, Y. Guo, Y. Guo, G. Lu, A. Baylet, A. Giroir-Fendler, Catalytic oxidation of vinyl chloride emission over $LaMnO_3$ and $LaB_{0.2}Mn_{0.8}O_3$ (B = Co, Ni Fe) catalysts, Appl. Catal. B 129 (2013) 509–516.
[22] S.-X. Chen, Y. Wang, A.-P. Jia, H.-H. Liu, M.-F. Luo, J.-Q. Lu, Enhanced activity for catalytic oxidation of 1,2-dichloroethane over Al-substituted $LaMnO_3$ perovskite catalysts, Appl. Surf. Sci. 307 (2014) 178–188.

[23] Y. Lu, Q. Dai, X. Wang, Catalytic combustion of chlorobenzene on modified LaMnO3 catalysts, Catal. Commun. 54 (2014) 114–117.
[24] K. Stephan, M. Hackenberger, D. Kießling, G. Wendt, Supported perovskite-type oxide catalysts for the total oxidation of chlorinated hydrocarbons, Catal. Today 54 (1999) 23–30.
[25] M. Alifanti, M. Florea, S. Somacescu, V.I. Parvulescu, Supported perovskites for total oxidation of toluene, Appl. Catal. B 60 (2005) 33–39.
[26] M. Richard, F. Can, D. Duprez, S. Gil, A. Giroir-Fendler, N. Bion, Remarkable enhancement of O_2 activation on yttrium-stabilized zirconia surface in a dual catalyst bed, Angew. Chem. Int. Ed. 53 (2014) 11342–11345.
[27] A. Giroir-Fendler, M. Alves-Fortunato, M. Richard, C. Wang, J.A. Díaz, S. Gil, C. Zhang, F. Can, N. Bion, Y. Guo, Synthesis of oxide supported $LaMnO_3$ perovskites to enhance yields in toluene combustion, Appl. Catal. B 180 (2016) 29–37.
[28] S. Cimino, S. Colonna, S. De Rossi, M. Faticanti, L. Lisi, I. Pettiti, P. Porta, Methane combustion and CO oxidation on zirconia-supported La, Mn oxides and $LaMnO_3$ perovskite, J. Catal. 205 (2002) 309–317.
[29] K. Stephan, M. Hackenberger, D. Kießling, G. Wendt, Supported perovskite-type oxide catalysts for the total oxidation of chlorinated hydrocarbons, Catal. Today 54 (1999) 23–30.
[30] K.-Z. Fung, T.-Y. Chen, Cathode-supported SOFC using a highly conductive lanthanum aluminate-based electrolyte, Solid State Ionics 188 (2011) 64–68.
[31] A. Dhahri, K. Horchani-Naifer, A. Benedetti, F. Enrichi, M. Ferid, Combustion synthesis and spectroscopic charaterisation of $LaAlO_3$ nanophosphors doped Er^{3+} ions, Ceram. Int. 39 (2013) 9613–9617.
[32] S. Dikmen, P. Shuk, M. Greenblatt, Hydrothermal synthesis and properties of Ce1–xLaxO2–δ solid solutions, Solid State Ionics 126 (1999) 89–95.
[33] S. Watanabe, X. Ma, C. Song, Characterization of structural and surface properties of nanocrystalline TiO2–CeO2 mixed oxides by XRD, XPS, TPR, and TPD, J. Phys. Chem. C 113 (2009) 14249–14257.
[34] A. Machocki, T. Ioannides, B. Stasinska, W. Gac, G. Avgouropoulos, D. Delimaris, W. Grzegorczyk, S. Pasieczna, Manganese—lanthanum oxides modified with silver for the catalytic combustion of methane, J. Catal. 227 (2004) 282–296.
[35] R. Craciun, B. Nentwick, K. Hadjiivanov, H. Knözinger, Structure and redox properties of MnO_x/yttrium-stabilized zirconia (YSZ) catalyst and its used in CO and CH_4 oxidation, Appl. Catal. A 243 (2003) 67–79.
[36] M. Wu, X. Wang, Q. Dai, D. Li, Catalytic combustion of chlorobenzene over Mn–Ce/Al_2O_3 catalyst promoted by Mg, Catal. Commun. 11 (2010) 1022–1025.
[37] H. Li, G. Lu, Q. Dai, Y. Wang, Y. Guo, Y. Guo, Efficient low-temperature catalytic combustion of trichloroethylene over flower-like mesoporous Mn-doped CeO_2 microspheres, Appl. Catal. B 102 (2011) 475–483.
[38] J. Zhu, Z. Zhao, D. Xiao, J. Li, X. Yang, Y. Wu, Study of $La_{2-x}Sr_xCuO_4$ (x = 0.0.5, 1.0) catalysts for NO + CO reaction from the measurements of O_2-TPD, H_2-TPR and cyclic voltammetry, J. Mol. Catal. A: Chem. 238 (2005) 35–40.
[39] B.P. Barbero, J.A. Gamboa, L.E. Cadús, Synthesis and characterisation of $La_{1-x}Ca_xFeO_3$ perovskite-type oxide catalysts for total oxidation of volatile organic compounds, Appl. Catal. B 65 (2006) 21–30.
[40] T. Nitadori, M. Misono, Catalytic properties of $La_{1-x}A'_xFeO_3$ (A′ = Sr,Ce) and $La_{1-x}Ce_xCoO_3$, J. Catal. 93 (1985) 459–466.
[41] E. Obeid, L. Lizarraga, M.N. Tsampas, A. Cordier, A. Boréave, M.C. Steil, G. Blanchard, K. Pajot, P. Vernoux, Continuously regenerating diesel particulate filters based on ionically conducting ceramics, J. Catal. 309 (2014) 87–96.
[42] Q. Dai, H. Huang, Y. Zhu, W. Deng, S. Bai, X. Wang, G. Lu, Catalysis oxidation of 1,2-dichloroethane and ethyl acetate over ceria nanocrystals with well-defined crystal planes, Appl. Catal. B 117–118 (2012) 360–368.
[43] A. Aranzabal, J.A. González-Marcos, M. Romero-Sáez, J.R. González-Velasco, M. Guillemot, P. Magnoux, Stability of protonic zeolites in the catalytic oxidation of chlorinated VOCs (1,2-dichloroethane), Appl. Catal. B 88 (2009) 533–541.
[44] S. Chatterjee, H.L. Greene, Y. Joon Park, Deactivation of metal exchanged zeolite catalysts during exposure to chlorinated hydrocarbons under oxidizing conditions, Catal. Today 11 (1992) 569–596.
[45] A. Aranzabal, M. Romero-Sáez, U. Elizundia, J.R. González-Velasco, J.A. González-Marcos, Deactivation of H-zeolites during catalytic oxidation of trichloroethylene, J. Catal. 296 (2012) 165–174.
[46] M. Gallastegi-Villa, A. Aranzabal, M. Romero-Sáez, J.A. González-Marcos, J.R. González-Velasco, Catalytic activity of regenerated catalyst after the oxidation of 1,2-dichloroethane and trichloroethylene, Chem. Eng. J. 241 (2014) 200–206.
[47] R. López-Fonseca, A. Aranzabal, J.I. Gutiérrez-Ortiz, J.I. Álvarez-Uriarte, J.R. González-Velasco, Comparative study of the oxidative decomposition of trichloroethylene over H-type zeolites under dry and humid conditions, Appl. Catal. B 30 (2001) 303–313.
[48] R. López-Fonseca, B. de Rivas, J.I. Gutiérrez-Ortiz, A. Aranzabal, J.R. González-Velasco, Enhanced activity of zeolites by chemical dealumination for chlorinated VOC abatement, Appl. Catal. B 41 (2003) 31–42.
[49] S. Scirè, S. Minicò, C. Crisafulli, Pt catalysts supported on H-type zeolites for the catalytic combustion of chlorobenzene, Appl. Catal. B 45 (2003) 117–125.
[50] P. Kim, Y. Kim, H. Kim, I.K. Song, J. Yi, Synthesis and characterization of mesoporous alumina for use as a catalyst support in the hydrodechlorination of 1,2-dichloropropane: effect of preparation condition of mesoporous alumina, J. Mol. Catal. A: Chem. 219 (2004) 87–95.
[51] E. Finocchio, C. Pistarino, S. Dellepiane, B. Serra, S. Braggio, M. Baldi, G. Busca, Studies on the catalytic dechlorination and abatement of chlorided VOC: the cases of 2-chloropropane, 1,2-dichloropropane and trichloroethylene, Catal. Today 75 (2002) 263–267.
[52] G. Sinquin, J.P. Hindermann, C. Petit, A. Kiennemann, Perovskites as polyvalent catalysts for total destruction of C1, C2 and aromatic chlorinated volatile organic compounds, Catal. Today 54 (1999) 107–118.
[53] D. Yu, W. Xingyi, L. Dao, D. Qiguang, Catalytic combustion of chlorobenzene over Mn–Ce–La–O mixed oxide catalysts, J. Hazard. Mater. 188 (2011) 132–139.